Surface Circulation Estimation Using Image Processing and Computer Vision Methods Applied to Sequential Satellite Imagery*

Abstract
Two methods of automating the process of ocean feature tracking for estimating surface currents in coastal areas are outlined. These methods involve pattern recognition and have certain advantages over the more familiar maximum cross-correlation technique of Emery et al. (1986). The first method requires three steps in its application–pattern selection, pattern recognition, and geometrical calculations–to determine both the cross- and the along-isotherm displacements. The second method calculates certain surface motion parameters, including rotation and translation in Hough parameter space. Each method is applied to sequential AVHRR IR satellite imagery off the U.S. east coast. Finally, some of the practical problems encountered in the application of these methods are described.

Introduction
Oceanographers and environmentalists need objective, rapid, and accurate methods to track features in satellite images in order to estimate surface circulation. Emery *et al.* (1986) adapted cloud motion algorithms to estimate sea surface velocity from AVHRR imagery. Their method demonstrated statistical reproducibility, but is time consuming and cannot determine the along-isopycnal transport or circular (rotational) velocities.

We have adopted pattern recognition methods to determine sea surface velocities. This methodology can potentially provide more and accurate information in the study of both cross- and along-isopycnal transport and allows the estimation of coherent surface velocity fields from a minimal set of observations. The models have been developed with computer vision and pattern recognition concepts, which involve artificial intelligence techniques. Briefly, a set of point correspondences, with shape invariance under motion, yields a set of parameters that carry the motion information. Several methods to obtain the motion of these parameters have been developed. Among these is the approach using Singular Value Decomposition, which proves to be very efficient. Similarly, the point or feature correspondence between im-

ages has been extensively studied in image processing in the area of temporal image compression using motion compensation. Two of these methods have been adapted to the sea surface motion framework and implemented with actual imagery off the U.S. east coast where eddies and other mesoscale ocean features often occur between the continental shelf and the Gulf Stream.

Many of the surface velocity estimates using feature tracking have been acquired along the U.S. west coast where the oceanic processes and features are quite different from those encountered along the U.S. east coast. Our initial efforts have focused on the Slope Water region just beyond the New York Bight where feature tracking has not been used extensively. We believe that the new pattern recognition methods will significantly improve our ability to determine actual velocity fields – both cross- and along-isopycnal transport – to determine the trajectory of oil spills, to carry out more effective search and rescue efforts, and to perform other environmental analyses of the surface flow in the region. The results of this research will also provide a better understanding of the sub-mesoscale circulation, therefore allowing us to obtain a better understanding of the physical processes in this coastal region, and improving our ability to use artificial intelligence techniques applied to remote sensing for coastal environmental studies.

In the following discussion, we present only a brief outline of these methods for automated features tracking, followed in each case by an example, i.e., pilot study, of their application. These methods will be described in greater detail in forthcoming studies.

Methodology

The Ordered Statistical Edge Detection Method
The method described in this section is a three-step process: pattern feature selection in using Ordered Statistical Edge Detection, pattern recognition and selection of the feature most closely matching the pattern feature from objects found in a search area in a subsequent image, and geometric calculations to compute cross and along frontal displacement direction and magnitude.

PATTERN FEATURE SELECTION
Assuming that surface thermal patterns are well-conserved over the typical periods between successive satellite images

Xiao-Hai Yan
Center for Remote Sensing, Graduate College of Marine Studies, University of Delaware, Newark, DE 19716.

Laurence C. Breaker
NOAA/NWS/National Meteorological Center, 5200 Auth Road, Camp Springs, MD 20746.

(~ 12 to 24 hours) (Vastano and Reid, 1985; Wahl and Simpson, 1990), it is possible to employ pattern recognition techniques to measure the displacement of features defined by surface temperature alone.
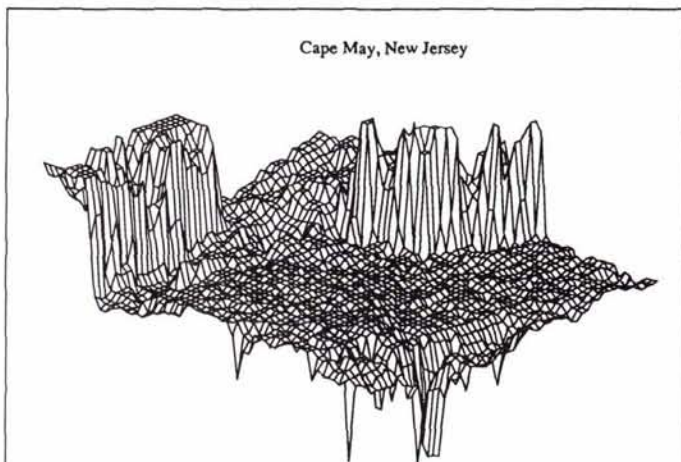
Edge detection can be employed initially to help select suitable features for tracking. This approach reduces the number of points selected, with a corresponding reduction in the number of required calculations. Figure 1 shows a 3D representation of the surface temperature field for the mouth of the Delaware Bay area. Feature selection maps this signal, discriminating against land, clouds, and other unwanted features. The high values correspond to land temperatures for Cape May, New Jersey, and the coast near Lewes, Delaware. The very low values in the lower right corner are light cumulus clouds. The water temperature signal varies considerably from the Delaware Bay (upper left, behind Cape May), to the ocean waters in the foreground.

The method uses an Ordered Statistical Edge Detection Algorithm (OSEDA) for feature selection (Hardie and Gnacek, 1990; Pitas and Venetsanopoulos, 1986; Holland and Yan, 1991), which effectively discriminates against noisy environments. This method is not orientation dependent, and it accurately detects ascending and descending gradients, identifying curved and linear features.

The OSEDA algorithm has been modified for our pilot study off the east coast to allow it to discriminate between ocean thermal gradient patterns and undesirable features such as cloud and land masses. These methods are not totally effective, but they do significantly reduce feature selection errors.

Mask parameters are determined from surface water temperatures and are applied in the area of interest. For selection of features away from land, masking is necessary only to avoid clouds. *Range* parameters provide a constraint for the maximum allowed change in apparent temperature.

Coastal areas, by definition, usually include land masses. The apparent temperatures for land features vary greatly due to diurnal heating and cooling. Linear classifiers for range and mask values allow use of coastal images, without time consuming preprocessing to screen unwanted features.

The edge detection method starts by evaluating data from a 5 by 5 edge detection tile (Figure 2). This results in selected tiles that are on gradients in regions of moderate temperature change, free from clouds and land. Tiles not selected are rejected if the temperature in the mapped area exceeds classification criteria. When an edge tile meets the modified OSEDA criteria, a pattern tile is mapped from an expanded area centered on the edge detection tile. The pixel values are rank ordered and compared with the mask values. If the high and low extreme mapped values fall within the mask values, the pattern tile is stored, the counter is incremented, and a *variable offset* is applied to allow spacing between the selected areas. This selection process continues until the search area is exhausted. For this study, we used an 11 by 11 pattern tile.

This method, in addition to being applied to the IR can also be adapted to visible and near-infrared band images by eliminating the mask value constraints. This allows tracking of slicks, plankton, ice flows or any other large visible feature of sufficient size which maintains its shape for at least 24 hours.

FEATURE RECOGNITION AND MATCHING IN SUBSEQUENT IMAGES

Once the initial image has been processed and pattern tiles have been selected, the second image is used for feature tracking. The size of the area to be searched for each selected
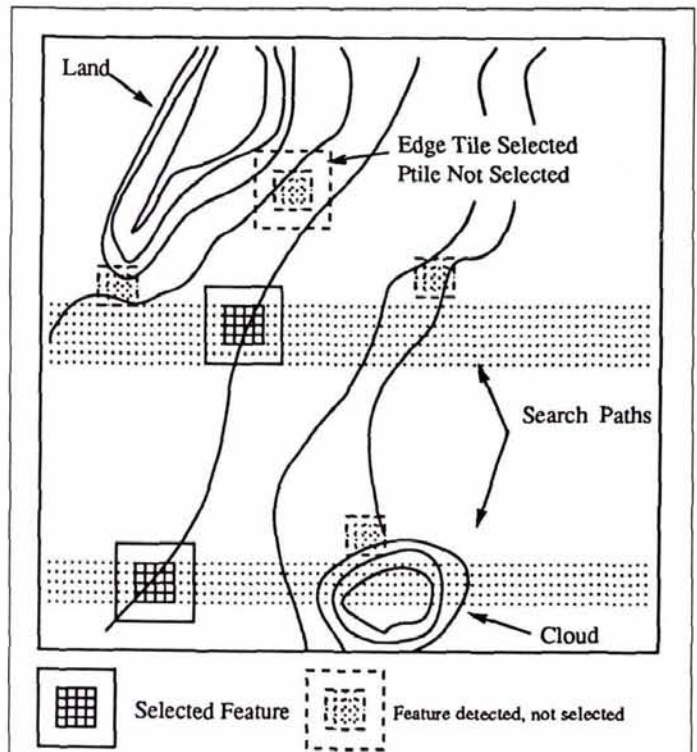

Thermal map: arbitrary scale, Azimuth: 315

Figure 1. Three-dimensional thermal signal map, 1258 hours local, 30 June 1989, Delaware Bay and coast. Clearly visible are the differences in signal between land, clouds, estuary, and coastal waters.

Figure 2. OSEDA feature selection and discrimination. An edge detection tile (5-by-5-pixel tile shown) moves incrementally across and down the search area to find features which meet range and mask criteria. Acceptable features are remapped to a specified pattern tile size. The expanded tile is accepted if it also meets the range and mask criteria.
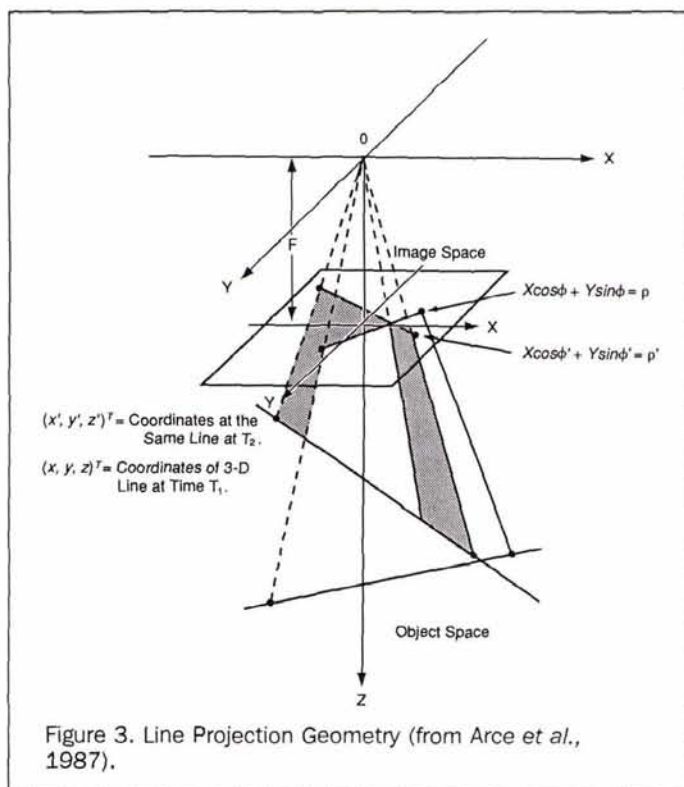
feature is governed essentially by the Bayes decision rule which involves the probabilities of finding an acceptable match (Fukunaga, 1990). Knowing that the selected features are altered over time by diffusion and rotation, and the displacement velocity varies greatly over short distances, the appropriate equation can be solved by limiting the area searched to a radius in which the feature can move during a sample interval. The problem then simplifies to one of linear mapping and classification, where subsequent pattern matching is dependent on a maximum-likelihood estimation.

When the search area is sampled, the features it contains must be evaluated in a way that produces the closest match to the pattern feature. This sorting is accomplished using classifiers to discriminate between features. The criteria used in this work are the statistical correlation of the pattern tile – search tile pair, limiting the root-mean-square (RMS) temperature variation between the search and pattern tiles, and limiting the pattern and search tile inter-temperature ranges. Selection of the matching feature is made by picking the feature which best matches the pattern tile using a basic branch and bound forward selection process.

Applying tile correlation in such a manner estimates the image spectrum in an auto-regressive fashion (Lim, 1990). The advantage of this method as a selection criteria is that it is less sensitive to background noise. In this one respect, the use of the correlation method to select matching features parallels the maximum cross-correlation approach of Emery et al. (1986).

Given intervals between images of 12 to 24 hours, it is almost certain that ocean thermal features rotate as well as translate. This is especially true in eddy flow areas. Methods exist (Rosenfeld, 1976) to transform the pattern tile array to different axis orientations. A single rotation transformation to allow for a left or right movement would increase computations by a factor of three.

When a full search tile area is mapped, it is correlated with the full pattern tile. For the results presented here, we used a minimum acceptable value for the correlation coefficient of 0.70. If the correlation criteria is met, the RMS difference of the tiles is evaluated to insure that the mean temperature change of the tile does not exceed a physically realistic maximum. This limit typically falls within the range of 3 to 5°C.

Error checks are required because the correlation coefficient is affected by spatial dislocation in all three dimensions. A search tile that is an exact match for the pattern tile in X and Y, can also vary in Z, or the temperature dimension, as well. A uniform change in temperature can yield a high correlation, but results in an erroneous selection. This occurs most commonly when land features or thin clouds are present in the search area of the subsequent image.

Selection of the best match occurs when a search area has been incrementally compared to the pattern tile. The area with the highest correlation to the pattern tile, which meets the classification criteria, is used to compute the surface flow.

One of our objectives is to reduce the number of calculations necessary to provide acceptable results. This is accomplished in part by using a reduced tile size search for pattern matching. A tile with dimensions equal to the edge detection tile will be first moved through the search area. A correlation between this tile and the center of the pattern tile will be made and compared to a threshold. The full search tile will be mapped only when the threshold is met or exceeded. This will result in a speed increase of approximately 75 percent when using a 5 by 5 reduced search tile and an 11 by 11 full search tile.

The ability of the OSEDA and constrained correlation methods to operate with images that contain land and clouds is a significant advantage. Of the more than 131 images examined for the Delaware coastal region from 1 March to 30 June 1989, only six pairs were sufficiently cloud-free in the area of interest to permit study. The OSEDA method, as presently implemented, is not adequate for screening images in an automated manner. Thin cloud layers can degrade the method, producing large numbers of false vectors. To evaluate large numbers of images for sufficiently open areas to permit processing, a more effective cloud screening method such as that of Simpson and Humphrey (1990) or Gautier et al. (1990) are required.

Estimating Sea Surface Motion Parameters in the Hough Parameter Space

Sea surface motion parameters can also be determined by the use of line correspondences in Hough parameter space. The method was extracted from Arce et al. (1987), in which the three-dimensional motion (rotation and translation) of a rigid planar patch is determined in Hough parameter space. For the general case of rotation and translation, the method involved solving for nine unknown parameters. Because we are only concerned with two-dimensional rotation and translation of ocean features on the sea surface, the equations of motion as employed by Arce et al. (1987) can be greatly simplified, such that there are only three unknown parameters that need to be determined.

BACKGROUND

The geometry of the problem is shown in Figure 3, where the object-space coordinates are denoted by lower-case letters and the image-space coordinates are denoted by upper-case letters. We assume that we are given two perspective views of the sea surface at two different times, t_1 and t_2. The coordinates at time t_2 are primed while the coordinates at time t_1 are not. The equations of motion are presented in three-di-

Figure 3. Line Projection Geometry (from Arce et al., 1987).

mensional space to preserve the methodology of Arce et al. (1987). From theoretical kinematics, any three-dimensional motion can be represented as a rotation about an axis through the origin followed by a translation. The coordinates at time t_2 are therefore related to those at t_1 by

$$\begin{pmatrix} x' \\ y' \\ z' \end{pmatrix} = \begin{pmatrix} r_{11} & r_{12} & r_{13} \\ r_{21} & r_{22} & r_{23} \\ r_{31} & r_{32} & r_{33} \end{pmatrix} \begin{pmatrix} x \\ y \\ z \end{pmatrix} + \begin{pmatrix} \delta x \\ \delta y \\ \delta z \end{pmatrix}, \quad (1)$$

where

$$\mathbf{R} = \begin{pmatrix} \cos\theta & -\sin\theta & 0 \\ \sin\theta & \cos\theta & 0 \\ 0 & 0 & 1 \end{pmatrix} \quad (2)$$

is the rotation matrix. θ is the angle of rotation around the axis in the positive sense from t_1 to t_2. Because we are only concerned with two-dimensional motion, the δz term in the above equation is 0 and $z = z'$. Finally, the coordinates at t_1 can be related to those at t_2 by

$$\begin{pmatrix} x \\ y \\ z \end{pmatrix} = \mathbf{R}^\mathrm{T} \begin{pmatrix} x' \\ y' \\ z' \end{pmatrix} - \mathbf{R}^\mathrm{T}\mathbf{T} \quad (3)$$

EQUATIONS OF MOTION
A parametric representation of a line in three-dimensional space can be represented by (referring to Figure 3)

$$\begin{pmatrix} x \\ y \\ z \end{pmatrix} = a \begin{pmatrix} v_1 \\ v_2 \\ v_3 \end{pmatrix} + \begin{pmatrix} k_1 \\ k_2 \\ k_3 \end{pmatrix} = a\mathbf{V} + \mathbf{K} \quad (4)$$

where $\mathbf{V} = (v_1, v_2, v_3)^\mathrm{T}$ is the directional vector, $\mathbf{K} = (k_1, k_2, k_3)^\mathrm{T}$ is the vector that translates the line, and a is a variable parameter. The v_3 term is reduced to 0 because of the two-dimensional restriction in our case. From the image-object relationship shown in Figure 3, the image space coordinates $(X,Y)^\mathrm{T}$ are related to the object-space coordinates $(x, y, z)^\mathrm{T}$ by

$$X = Fx/z, \qquad Y = Fy/z.$$

From the above, $X = F(av_1 + k_1)/(av_3 + k_3)$, $Y = F(av_1 + k_1)/(av_2 + k_2)$. Combining the above equations, we obtain the image-space line equation

$$X \cos\Phi + Y \sin\Phi = pF, \quad (5)$$

where Φ is the angle between a normal to the line and the positive X axis, and p is the signed distance along the normal from the origin to the line. The terms p and Φ are often referred to as the Hough parameters, and they uniquely represent a line in two dimensions. After three-dimensional rotation and translation, the parametric line representation can be expressed as

$$\begin{pmatrix} x' \\ y' \\ z' \end{pmatrix} = a\mathbf{R} \begin{pmatrix} v_1 \\ v_2 \\ v_3 \end{pmatrix} + \mathbf{R} \begin{pmatrix} k_1 \\ k_2 \\ k_3 \end{pmatrix} + \begin{pmatrix} \delta x \\ \delta y \\ \delta z \end{pmatrix} = a\mathbf{V}' + k'. \quad (6)$$

The rotated and translated three-dimensional line is then projected onto the image-space line, resulting in an expression of the following from

$$X \cos\Phi + Y \sin\Phi' = p'F, \quad (7)$$

To simplify the results, the following relations are constructed:

$$\tau_1 = \tan\Phi = \frac{k_3v_1 - k_1v_3}{k_2v_3 - k_3v_2} \qquad \tau_2 = \frac{pF}{\cos\Phi} = \frac{k_2v_1 - k_1v_2}{k_2v_3 - k_3v_2}.$$

After the motion, these parameters are τ_1' and τ_2'. Thus, we can express the above as

$$\begin{aligned} X + Y\tau_1 &= \tau_2, \\ X + Y\tau_1' &= \tau_2' \end{aligned} \quad (8)$$

Here τ_1^{-1} is the slope and τ_2 is the X intercept of the image-space line. Therefore τ_1 and τ_2 uniquely determine an image-space line and can be thought of as Hough parameters. Thus, τ_1 and τ_2 represent the Hough parameters of a line that represents a sea-surface temperature gradient in the first satellite image while τ_1' and τ_2' represent that same line in the second image. The equations of motion in turn can be solved for rotation, translation, or both rotation and translation. For the general case of both rotation and translation, the governing matrix is

$$\begin{pmatrix} -\tau_1' & -\tau_1\tau_1' & \tau_1'\tau_2 & 1 & \tau_1 & -\tau_2 & 0 & 0 & 0 \\ -\tau_2' & -\tau_1\tau_2' & \tau_2\tau_2' & 0 & 0 & 0 & -1 & -\tau_1 & \tau_2 \end{pmatrix} \mathbf{P}_g = 0. \quad (9)$$

where the matrix $\mathbf{P}_g$ is a column vector containing appropriate sine and cosine functions. In this particular case there are three unknowns and two equations. An additional two equations can be utilized by using two line correspondences. The two lines used in this method would have to originate from the same rigid planar patch and would thus have to undergo the same translation and rotation.

Results

Application to the Delaware Coastal Region
Surface, subsurface, and bottom currents in the Delaware coastal region have been extensively studied (Münchow et al., 1990). Figure 4 shows the locations for 21 moored buoys used during this study. From these buoys, mean current for depths between 5 and 10 metres were obtained. Satellite observations acquired during this study have been correlated with these observations.
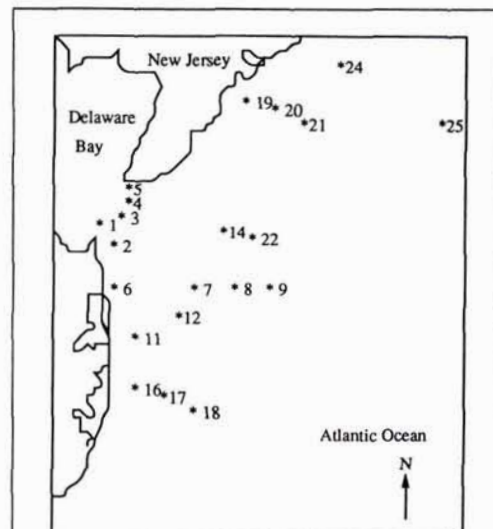

Figure 4. Selected anchored buoy locations for the Delaware coastal region, which were used to evaluate accuracy of satellite derived surface currents (from Münchow et al., 1990).
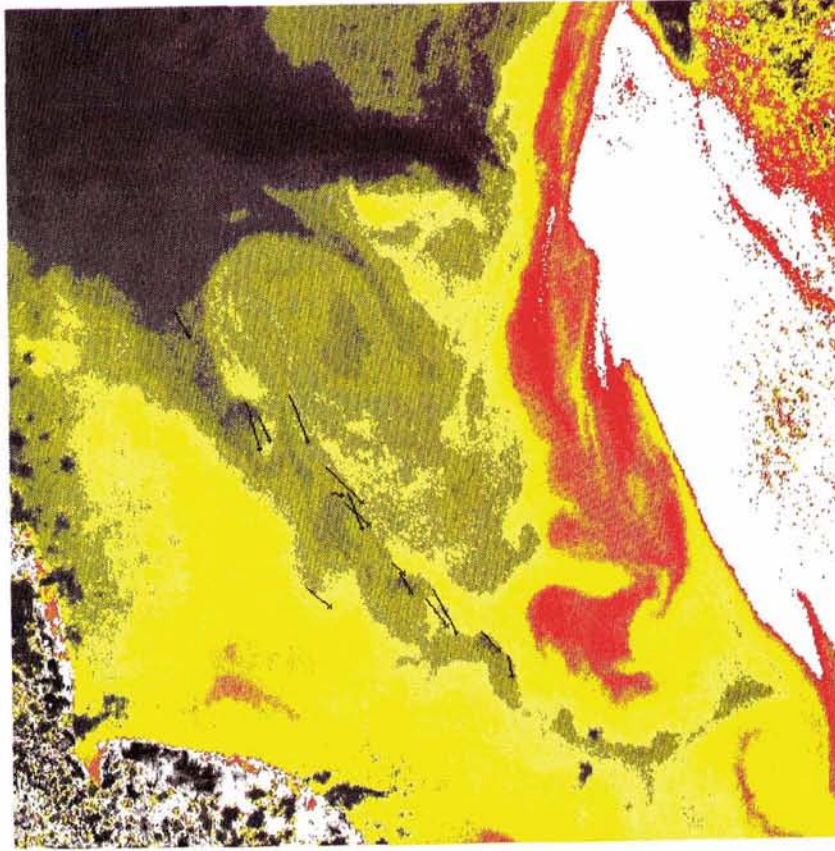
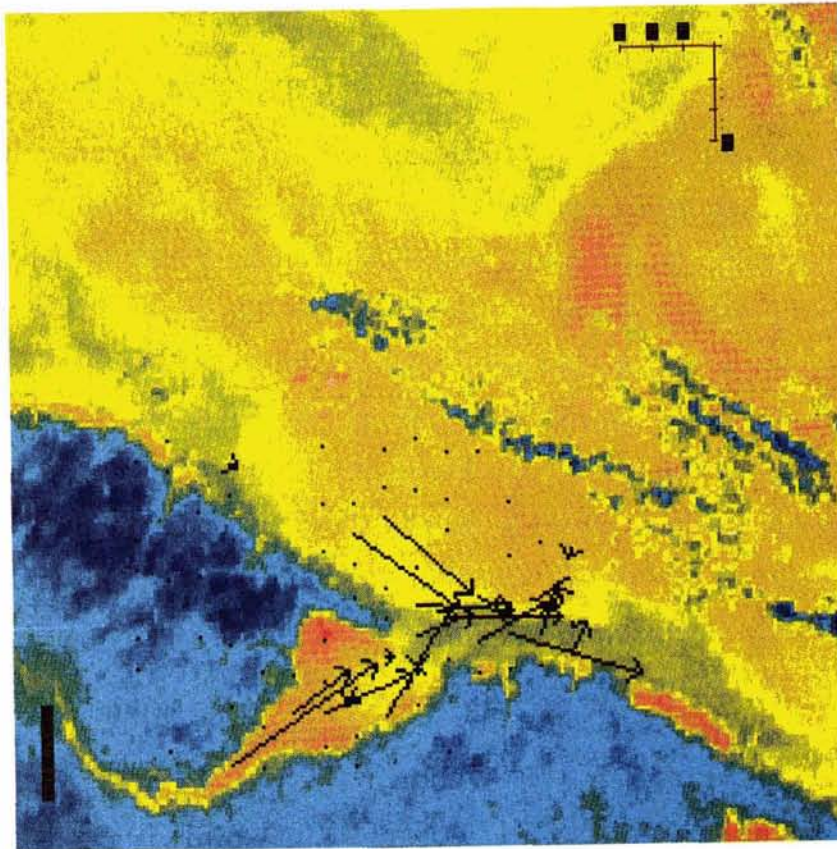Plate 2. The velocity vectors computed from the image of 24 June 1991.

Plate 1. Surface current vectors for the Delaware Bay - New Jersey coastal region, for a 12-hour period, 30 June 1989.

TABLE 1. MEAN SATELLITE OBSERVATIONS FOR SELECTED COASTAL DELAWARE AND NEW JERSEY IN SITU BUOYS. VALUES WERE DETERMINED BY MATCHING SATELLITE DERIVED VECTOR ORIGINS WITH BUOY POSITIONS. THE VALUES LISTED ARE THE MEANS OF MULTIPLE OBSERVATIONS FOR EACH LOCATION.

	Mean satellite - buoy observations	
Mooring	Axis degrees	Velocity cm/s
1	131.02	112.80
4	134.37	36.75
5	159.86	79.00
6	116.45	34.00
7	90.00	27.0
9	174.34	12.50
11	108.43	42.00
12	165.85	26.00
14	180.19	32.33
16	92.33	26.00
17	111.07	27.00
18	117.96	23.67
19	217.46	12.50
20	193.28	18.50
21	168.74	16.40
22	146.48	40.00
24	164.52	10.50

Observations from March 1989 show that SSTs in, and beyond, the bay range from 3.25° to 7.62° C. Applying the OSEDA to these data, of the 31 pattern tiles selected, 16 found no reduced set search tiles that met the correlation criteria. The remaining 15 tiles resulted in 79 to 137 full tiles, but none produced a correlation >0.50. The low correlation suggests a very deep mixed layer due to cooling at the surface, which precludes features which are sufficiently persistent to be matched in subsequent images. The vertical diffusion condition ($\partial T/\partial z \ll \partial T/\partial x$) is apparently not met here due to continuous vertical mixing of surface and subsurface (> 50 meters) waters.

Images from late May and early June 1989 produced acceptable results once the SST reached values greater than 12.6° C offshore by 28 May. At an SST of 12.6° C, results were obtained from only 49 pattern tiles. By 10 June, the SST offshore had reached 16.13° C, yielding results in approximately 75 percent of the cases.

Plate 1 shows the surface flow in the Delaware coastal region for 30 June 1989. Three images were available for this period and were processed as two pairs. Search tile matching was hampered by thin clouds which frequently moved into the offshore region. The SST was high for the bay (21.38° C), and 20.5° C for the offshore area.

Verifying the displacement of surface thermal features to infer in situ surface currents was accomplished by comparing the OSEDA-derived vectors with in situ buoy data. Eight image pairs from the period 28 May - 30 June 1989 produced

TABLE 2. COASTAL DELAWARE AND NEW JERSEY SATELLITE - BUOY DIRECTION AND SPEED COMPARISON.

Mean satellite - buoy comparison	
Parameter	Result
Direction Correlation	0.83
Std. Deviation (σ_{Az})	20.45°
Mean Error	−4.38°
Speed Correlation	0.96
Std. Deviation (σ_V)	7.76 cm/s
Mean Error	−7.75 cm/s

110 vectors that could be matched to 17 buoys. Means for each station were computed and are listed in Table 1. These values were then correlated with the in situ data.

The results obtained were compared to the mean M_2 tidal measurements of Münchow et al. (1990). These results were assumed to represent the average movement, because the M_2 tide is the dominant component of the surface flow field in this coastal region.

The agreement in velocity between the satellite and buoy measurements is encouraging with a σ_v of 8 cm/s over a range from 9 to 112 cm/s.

Slope Water Region

A portion of the slope water region off the U.S. east coast between 37° N and 41° N was also examined in this study. This region is also an area of interest to NOAA's CoastWatch Program. AVHRR satellite data are readily available for this area. The circulation in this region is dominated by the southwestward flow of relatively fresh water from the Labrador Current. Generally, the surface currents in this region are weak and variable but tend to flow more-or-less parallel to the Gulf Stream but in the opposite direction. The flow is frequently disturbed by anticyclonic warm-core eddies which entrain waters from the Gulf Stream and the Sargasso Sea.

Another prominent feature in the slope water region is the shelf/slope front which is located along the outer continental shelf. This front typically overlies the continental shelf break (Mooers et al., 1978). It forms the transition between shelf waters near the coast and the slope waters further offshore (Beardsley and Flagg, 1975). Breaker et al. (1992) used an interactive feature-tracking method to analyze satellite AVHRR data from 24 and 25 June 1991. Surface velocities ranged from about 4 to 33 cm/sec. Using the second automatic feature-tracking method involving line correspondences in Hough parameter space and the same satellite data, we computed a velocity field in the same region. The velocities we compute range from 5 to 30 cm/sec. A lagrangian trajectory from a satellite-tracked drifter is shown in Figure 5. We have computed velocity vectors using points near this drift route and the results are shown in Plate 2. The mean direction we computed is about 239°, which appears to be in a close quantitative agreement with those directions from drifter direction measurement.

Conclusions

Although the automatic method of satellite feature tracking for estimating surface currents has not been applied extensively to the east coast regions considered here, the results of this study do indicate that reasonable values for surface velocity (speed and direction) can be obtained . These results generally compare favorably with other oceanographic analyses for this region.

The results of this study provide a starting point for developing operational procedures to estimate time dependent surface currents. Surface current velocities are required over large coastal regions for estimating the drift and dispersion of oil slicks, ocean dumped wastes, and run-off into estuaries. Until recently such studies required cumbersome drogue and dye tracking techniques including ships and aircraft (Klemas, 1980).

The new pattern recognition methods indicated here may potentially improve our ability to determine the fate of various types of pollution, to calculate actual flow fields — both cross and along-isopycnal transports, to define the trajectory of oil spills, to carry out more effective search and rescue efforts, and to perform other environmental analyses of estuarine and coastal waters. These techniques may also provide a better understanding of sub-mesoscale circulation
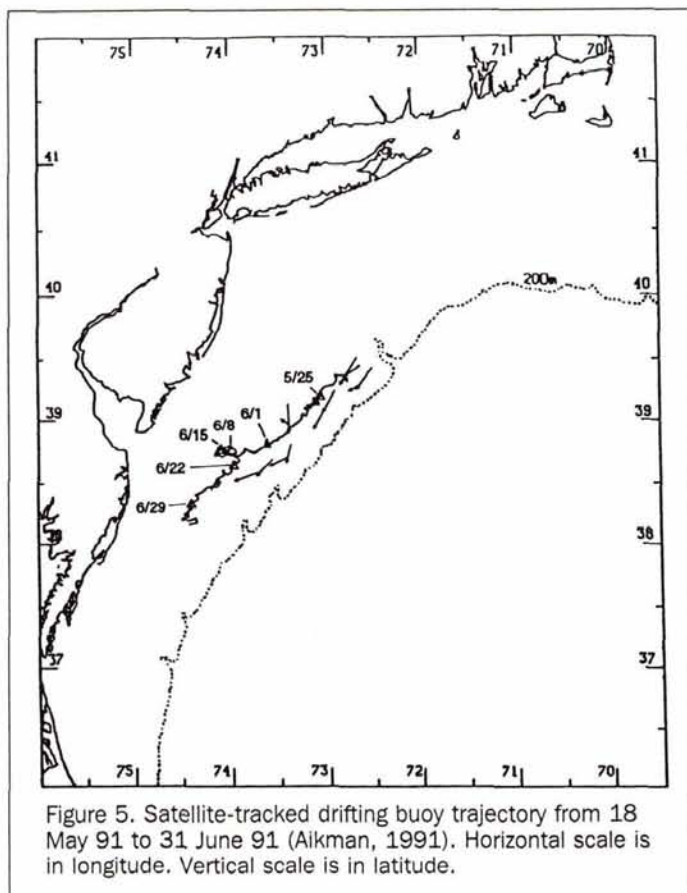
Figure 5. Satellite-tracked drifting buoy trajectory from 18 May 91 to 31 June 91 (Aikman, 1991). Horizontal scale is in longitude. Vertical scale is in latitude.

features, therefore potentially providing a better understanding of the physical processes in various coastal regions, and to improve our ability to use state-of-the-art technology, including artificial intelligence, pattern recognition, and remote sensing in coastal environmental studies.

Acknowledgments

References

Arce, G. R., W. E. Wonchoba, and E. R. Malaret, 1987. Estimating the three-dimensional motion of a rigid planar patch in the Hough parameter space, Internal Report presented at the SPIE Conference on Advances in Intelligent Robots and Computer Vision, Cambridge, Massachusetts, 5 Nov.

Beardsley, R. C., and C. N. Flagg, 1975. The water structure, mean currents, and shelf/slope water front of the New England continental shelf, *Proceedings of 7th Liege Colloquium on Ocean Atmosphere*, 10:209–226.

Breaker, L. C., L. D. Burroughs, T. B. Stanley, and W. B. Campbell, 1992. *Estimating Surface Currents in the Slope Water Region between 37 and 41°N Using Satellite Feature Tracking*, National Meteorological Center, Report OPC Contribution No. 48.

Emery, W. J., A. C. Thomas, M. J. Collins, W. R. Crawford, and D. L. Mackas, 1986. An objective method for computing advective surface velocities form sequential infrared satellite images, *Journal of Geophysical Research*, 91:12,865–12,878.

Fukunaga, K., 1990. *Intro. to Statistical Pattern Recognition*, 2nd Ed., Academic Press, San Diego.

Gautier, C., G. Diak, and S. Masse, 1990. A simple physical model to estimate incident solar radiation at the surface from GOES satellite data, *Journal of Applied Meteorology*, 19:1005–1012.

Hardie, R. C., and R. Gnacek, 1990. *Robust Ranked - Order Based Vector Edge Detectors for Color Image Processing*, Internal Report, Dept. of Electrical Engineering, University of Delaware, Newark, DE, April.

Holland, J., and X.-H. Yan, 1991. Remote sensing estimation of surface flow in the Delaware and New Jersey coastal region, *EOS*, 72(17):155.

Klemas, V., 1980. Remote sensing of coastal fronts and their effects on oil dispersion, *Int. J. Remote Sensing*, 1(1):11–28.

Lim, J. S., 1990. *Two - Dimensional Signal and Image Processing*, Prentice-Hall, Englewood Cliffs, N.J.

Mooers, C. N. K., C. N. Flagg, and W. C. Boicourt, 1978. Prograde and retrograde fronts, *Oceanic Fronts in Coastal Processes* (M. Bowman and W. Esaias, editors), Springer-Verlag, New York, pp. 43–58.

Münchow, A., A. K. Masse, and R. W. Garvine, 1990. Astronomical and nonlinear tidal currents in a coupled estuary shelf system. *Continental Shelf Research*, in press.

Pitas, I., and A. N. Venetsanopoulos, 1986. Nonlinear order statistic filters for image filtering and edge detection, *Signal Processing*, 10:395–413.

Rosenfeld, A., 1976. *Digital Picture Analysis*, Springer-Verlag, New York.

Simpson, J. J., and C. Humphrey, 1990. An automated cloud screening algorithm or daytime advanced very high resolution radiometer imagery, *Journal of Geophysical Research*, 95(C8):13,459–13,481.

Vastano, A. C., and R. O. Reid, 1985. Sea surface topography estimation with infrared satellite imagery, *Journal of Atmospheric and Oceanic Technology*, 2:393–400.

Wahl, D. D., and J. J. Simpson, 1990. Physical processes affecting the objective determination of near-surface velocity from satellite data, *Journal of Geophysical Research*, 95(C8):13,511–13,528.